Photothermia and Activated Drug Release of Natural Cell Membrane Coated Plasmonic Gold Nanorods and β-Lapachone

Valeria S. Marangoni,[†] Juliana Cancino Bernardi,[†] Ianny B. Reis,[‡,§] Wagner J. Fávaro,[‡,§] and Valtencir Zucolotto*,[†]

[†]Nanomedicine and Nanotoxicology Group, Physics Institute of Sao Carlos, University of São Paulo, São Carlos, BR-13560970, Brazil

[‡]Laboratory of Urogenital Carcinogenesis and Immunotherapy, Department of Structural and Functional Biology, and [§]NanoBioss, Institute of Chemistry, University of Campinas (UNICAMP), Campinas, São Paulo 13083-970, Brazil

S *Supporting Information*

ABSTRACT: Plasmonic gold nanoparticles present extraordinary potential for near-infrared photothermal and triggered-therapeutic release treatments of solid tumors. In this study, we create a multifunctional nanocarrier in which PEG-coated gold nanorods are grouped into natural cell membrane vesicles (CM) from lung cancer (A549) cells and loaded with β-lapachone (CM-β-Lap-PEG-AuNRs). β-Lapachone (β-Lap) is an anticancer agent activated by the enzyme NADP(H):quinine oxidoreductase (NQO1), commonly found at higher levels in cancer cells. The irradiation with near-infrared (NIR) laser leads to disruption of the vesicles and release of the PEG-AuNRs and β-Lap. The system presents an enhanced in vitro cytotoxicity against A549 cancer cells, which can be attributed to the specific cytotoxicity of β-Lap combined with heat generated by laser irradiation of the AuNRs. In agreement, in vivo treatment with CM-β-Lap-PEG-AuNRs and irradiation shows a histopathological recovery from nonmuscle invasive bladder cancer of most of the animals with only one cycle of application and irradiation. Such multifunctional platform is a promising candidate for improved activated drug release and phototherapy.

KEYWORDS: *phototherapy, drug delivery, nanomedicine, cell membrane, gold nanorods*
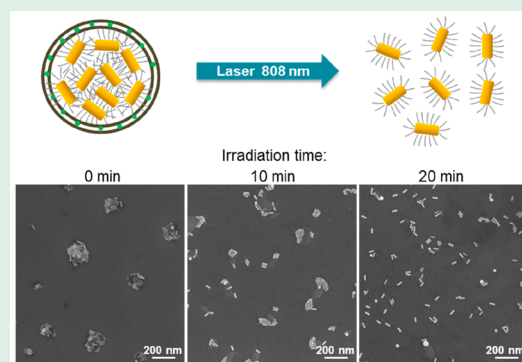
1. INTRODUCTION

Nanomaterials have found promising applications in medicine, especially in cancer, in which nanomaterials have revolutionized diagnosis and treatment strategies. As example, plasmonic photothermal therapy (PPTT), which consists in the transduction of light by specific nanosystems into heat, has emerged as a potential minimally invasive alternative for cancer treatment with reduced side effects.[1] The use of long-wavelength laser irradiation, such as in the near-infrared region (NIR) between 650 and 950 nm, is particularly advantageous because it exhibits the maximum radiation penetration into tissues and can be used in deeply seated targets.[2] Gold nanorods (AuNRs) provide excellent systems for applications in PPTT because of their localized surface plasmon resonance (SPR) at NIR.[3,4] Recently, multifunctional systems for combined chemical and phototherapy have emerged as a potential platform for cancer therapy. It has been demonstrated that the heating caused by phototherapy may increase susceptibility of cancer cells to other treatments, resulting in an improved therapeutic efficacy compared with chemo or photothermal therapy alone.[5,6] However, despite many studies in this area, the low accumulation rate of the nanoparticles in the target tissue is still a challenge.[7]

To enhance the accumulation of nanoparticles in the tumor, new strategies of functionalization of the nanomaterials have been developed. Among them, the coating with natural cell membranes has proved to be an interesting alternative to camouflage the particles and extend their blood circulation time.[8−12] This strategy has been extended to cancer cells, demonstrating higher specificity for cancer cell targeting[13] and also potential for cancer immunotherapy.[14] Recently, a cooperative membrane-targeting using extracellular vesicles from cancer cells have been explored to enhance the accumulation and distribution of therapeutic agents in the tumor.[15] The use of reconstructed stem cell membranes as platform for drug delivery[16] and imaging and photophotherapy of tumors[17] have also been reported. They can exhibited many favorable properties such as efficient drug loading, biocompatibility, and prolonged blood circulation time.[18,19]

In this study, we developed a multifunctional nanocarrier for photothermal therapy and drug delivery. In this nanotheranostic system, PEG-coated gold nanorods were grouped
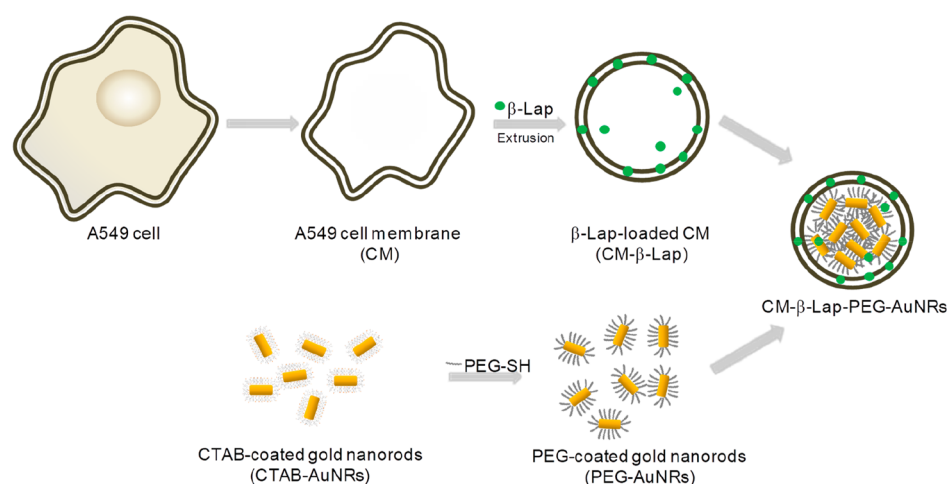
Figure 1. Schematic representation (not to scale) of proposed mechanism for the fabrication of the cancer cell membrane-coated PEG-gold nanorods and loaded with the anticancer agent β-Lapachone (CM-β-Lap-PEG-AuNRs). First, A549 lung cancer cells are isolated, lysed to remove the internal content, and purified by ultracentrifugation. β-Lap is loaded on cell membrane structure and they are extruded through 200 nm porous membrane (CM-β-Lap). In parallel, gold nanorods (AuNRs) are synthesized by the seed-mediated method in the presence of surfactant CTAB, followed by covalent functionalization with mPEG-SH. The fusion of the resulting PEG-AuNRs and CM-β-Lap are performed by mechanical extrusion through 100 nm pore membrane.

into natural cell membrane vesicles from lung cancer cell membranes (A549) and loaded with the anticancer drug β-lapachone (CM-β-lap-PEG-AuNRs). β-lapachone cytotoxicity is activated by NADP(H):quinine oxidoreductase (NQO1), an enzyme overexpressed in many human cancers.[20] Consequently, it presents very low toxicity to normal cells and can be used as an effective and selective antitumor agent. However, its poor solubility, low stability in circulation, short blood circulation time, and poor specificity led to low tumor accumulation and have limited its therapeutic applications.[21] Therefore, substantial efforts have focused on its incorporation in nanostructured systems.[22,23]

Our aim was to develop a specific multifunctional system for cancer treatment by using the antigens and the unique properties of the cell membrane combined with photothermal properties of AuNRs and anticancer activity of β-lap. In particular, we have chosen the A549 cell line, because of its metastatic character which may consequently, make it a good candidate to enhance delivery to cancer and their metastatic sites. The platform was characterized by spectroscopy and electron microscopy techniques and their properties in the presence and absence of a NIR laser both in vitro and in vivo were investigated. The system described here differs from others cell-membrane encapsulated nanomaterials mainly due to the NIR-activated synergic toxicity demonstrated between the heat generated by laser irradiation and β-lapachone.

2. RESULTS AND DISCUSSION

2.1. Gold-Nanorod-Loaded Cancer Cell Membrane Fabrication. An overview on the different steps of the fabrication of the CM-β-Lap-PEG-AuNRs is shown in Figure 1. First, the A549 cancer cell membranes (CM) were extracted and purified by ultracentrifugation, followed by incorporation of the anticancer agent β-Lap. Because of the hydrophobic behavior of the β-Lap molecules, it is expected that most of them are associated together with the lipid compartments of the vesicle (green points in Figure 1). The gold nanorods were fabricated by the seed-mediated method in the presence of CTAB and covalently functionalized with mPEG-SH. The

fusion of the PEG-AuNRs and CM-β-Lap were performed by mechanical extrusion through 100 nm pore membrane.

Cancer cell membrane vesicles (CM) were derived from A549 cancer cells. The reasoning for choosing this cell line as a source lies in their metastatic ability.[24] Cell-membrane-based systems exhibit natural properties and some biofunctions from their parent cells.[25] Taking advantage of the inherent homotypic binding capability among tumor cells[13] and the metastatic characteristic of the A549 cells,[24] their derived membrane vesicles seem to be good candidates for enhance drug and nanoparticle delivery to the cancer and their metastatic sites. The qualitative analysis of the cell membrane proteins was performed by polyacrylamide gel electrophoresis (SDS-PAGE), as shown in Figure S1. The resulting vesicles appear to retain the critical cell membrane proteins.[13] The presence of specific and tumor-associate antigens from the source cancer cell line in the derivate vesicles have been confirmed in a previous study performed by Fang et al.[13] Quantitative BCA analysis was used to calculated the total protein concentration. Phospholipids were found to be the most abundant lipid class present in the A549 cell membrane vesicle according to the latroscan TLC/FID analysis (Figure S2).

The loading of β-Lap into the CM structure was performed by incubation of the CM with β-Lap, followed by extrusion and dialysis. The hydrodynamic diameter measured by dynamic light scattering (DLS) after extrusion confirms the formation of vesicles with an average diameter around 150 nm (Figure S1B). Figure S1C shows a comparison of the UV−vis spectra of the CM before and after the loading of β-Lap. The CM spectrum presents a small absorption band at ca. 260 and 220 nm, which came from the proteins of the membrane. After loading the β-Lap, the spectrum exhibited a typical β-Lap absorption peak at 257 nm.

PEG-AuNRs, with an average aspect ratio (length/width) of approximately 3.5 (Figure S3), were fused with the CM-β-Lap derived vesicles through mechanical extrusion upon coextrusion of CM-β-Lap and PEG-AuNRs through a 100 nm polycarbonate membrane for several times. The CM-β-Lap/
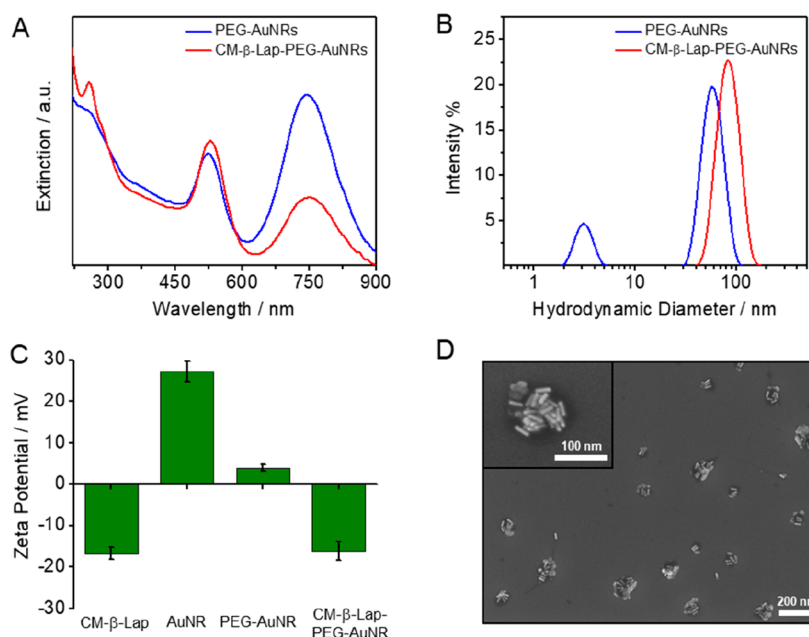
Figure 2. Characterization of gold nanorods coated with cell-membrane-loaded β-lapachone (CM-β-Lap-PEG-AuNRs). (A) UV−vis−NIR spectra, (B) hydrodynamic diameter obtained from DLS measurements and (C) Zeta Potential of PEG-AuNRs before and after coating with CM-β-Lap; (D) SEM images of CM-β-Lap-PEG-AuNRs showing the PEG-AuNRs grouped inside the cell membrane vesicles.
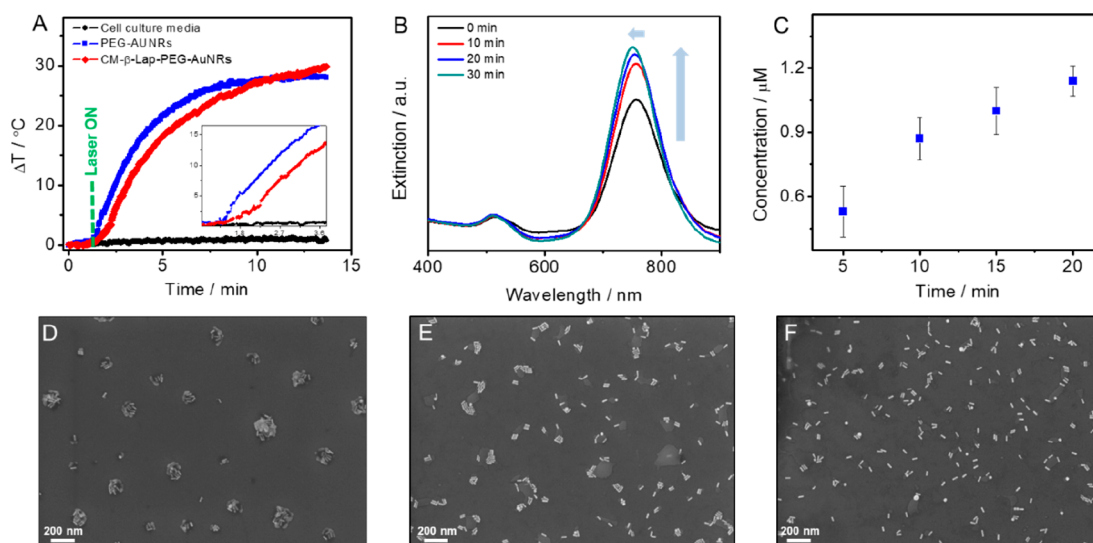
Figure 3. (A) Representative of temperature change *vs* time in suspensions (optical density at 750 nm = 1) irradiated with 808 nm laser with power density of 1.5 Wcm^{-2}. (B) Increase in the longitudinal band with the laser irradiation and (C) release of β-lapachone at different time of irradiation for CM-β-Lap-PEG-AuNRs. SEM images of CM-β-Lap-PEG-AuNRs (D) before, (E) after 10 min, and (F) after 20 min of laser irradiation. The laser irradiation increases the temperature of the suspension, breaks the vesicles, and causes the release of the AuNRs.

PEG-AuNR ratio was varied to adjust the uniformity of the system and to avoid free AuNRs. The total concentration of β-Lap in the final conjugates (OD$_{750\ nm}$ = 0.6) was around 2.5 μM, which revealed a low loading efficiency. The low β-lap loading efficiency has also been observed in β-lap-loaded micelles and polymeric particles.[22]

A comparison of the UV−vis−NIR spectra of PEG-AuNRs before and after the conjugation is shown in Figure 2A. A slightly red shift is observed in the presence of the membrane and indicates the changing in the dielectric nature surrounding the nanorods.[26] More pronounced, however, is the changing in the intensity of the longitudinal plasmonic peak, which was significantly reduced. This effect has been attributed to the

plasmon coupling effect, which is typically induced by gold nanorods assembly.[27] A comparative analysis of the hydrodynamic diameter of PEG-AuNRs with/without CM-β-Lap by DLS measurements is shown in Figure 2B. Before the fusion, the PEG-AuNRs presented two different size distributions, which is consistent with their anisotropic shape, whereas the final CM-β-Lap-PEG-AuNRs presented only one size distribution around 100 nm. Zeta potential measurements further confirmed the encapsulation (Figure 2C). The cell membrane presented a negative charge, due to the presence of phospholipids and proteins. The zeta potential of AuNRs changed from highly positive (due to the presence of CTAB molecules) to close to zero after PEGylation, and to negative
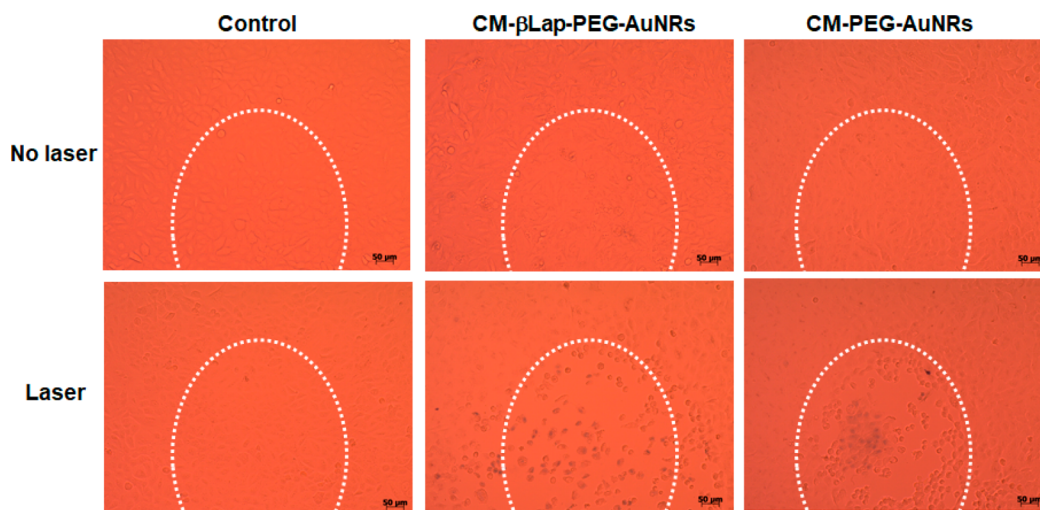
Figure 4. Photothermal therapy of A549 cancer cells treated with CM-β-Lap-PEG-AuNRs and CM-PEG-AuNRs. The highlight areas represent approximately the laser spots ($\sim$1.5 W cm^{-2}, 10 min) on the samples. Dead cells were stained with Trypan Blue. Cells without the particles (control) are not affected by the laser irradiation, whereas cells incubated with CM-β-Lap-PEG-AuNRs and CM-PEG-AuNRs were visibly injured.

upon fusion with CM-β-Lap, suggesting a successful coating. The SEM image (Figure 2D) clearly shows that the AuNRs are grouped and the average diameter of the final system, called here as CM-β-Lap-PEG-AuNRs, was approximately 109 nm (Figure S4). In the serum stability analysis (Figure S5), none major change was observed, indicating the CM-β-Lap-PEG-AuNRs present good stability either in buffer or in biological media.

The ability of CM-β-Lap-PEG-AuNRs to avoid the binding of proteins from the biological media was evaluated by Isothermal titration calorimetry (ITC) (Figure S6). The interactions between bovine serum albumin (BSA), a major representative globular protein present in the serum, and PEG-AuNRs, CM-β-Lap-PEG-AuNRs, and CTAB/PEG-AuNRs were evaluated. CTAB/PEG-AuNRs resulted from PEGylation of the CTAB-AuNRs using a lower concentration of mPEG-SH, i.e., just enough to keep the particles stable in 0.1x PBS, resulting in a final zeta potential of +18 mV. In the tested conditions, no heat exchange was observed for PEG-AuNRs and CM-β-Lap-PEG-AuNRs, while the binding between BSA and CTAB/PEG-AuNRs was an exothermic process (Figure S6). It is expected that the PEGylation of nanoparticles would reduce protein adsorption on the nanoparticle because of the steric repulsions and hydrophilization induced by PEG chains. Previous studies have also shown no heat exchange when BSA is added to PEGylated nanoparticles.[28,29] Because the CM-β-Lap-PEG-AuNRs presented a similar behavior of PEGylated particles, we can infer that they can also avoid BSA binding.

2.2. NIR Irradiation Led to Disruption of the Vesicles and Release of the AuNRs and β-Lap. Photothermal therapy has been increasingly investigated as a minimally invasive alternative for cancer treatment.[1] We investigated the photothermal properties of the CM-β-Lap-PEG-AuNR system using a 808 nm laser at a power density of 1.5 W cm^{-2}, which is consistent with earlier experimental conditions used in PPTT to guarantee minimal side effects.[30] After the irradiation, the temperature of both systems CM-β-Lap-PEG-AuNRs and PEG-AuNRs increased (Figure 3A). Considering the decreasing of the AuNR absorption in the NIR region after their incorporation in the cell membrane (Figure 2A), we can infer that the photothermal efficiency is lower for CM-β-Lap-PEG-

AuNRs compared to the PEG-AuNRs. Also, a closer examination revealed some slight difference mainly in the initial period (inset of Figure 3A). The curve slope in the first minutes was greater for PEG-AuNRs than CM-β-Lap-PEG-AuNRs. However, after ca. 2.5 min, the signals seem almost the same. This could be ascribed to the assembly of nanorods in the CM-β-Lap-PEG-AuNR system. Initially, the AuNRs are grouped inside the CM vesicles, which decrease their absorption at NIR region. The temperature increase generated by the laser irradiation destabilize the cell membrane structure and release both PEG-AuNRs and β-Lap, and as they are being released, their photothermal behavior is becoming more likely the free PEG-AuNRs. The CM-β-Lap-PEG-AuNRs also take more time to stabilize at the final temperature, which suggests that changes in their structure still happen even after 10−15 min of irradiation. No significant temperature change was observed when cell culture media were irradiated with the NIR laser at the same conditions.

In the heating and cooling analysis (Figure S7), the CM-β-Lap-PEG-AuNR suspension was irradiated for 25 min, then the laser was turned off until temperature stabilization, and again turned on. In the second heating step, only one curve slope and a faster stabilization were observed, suggesting that the PEG-AuNRs are not grouped anymore. This hypothesis is confirmed by the FEG-SEM images before and after 10 and 20 min of laser irradiation (Figure 3D−F), where it may be seen the gradual release of the PEG-AuNRs from the CM vesicles upon laser irradiation. It is worth stressing that the laser irradiation did not cause any shape modification, in size or morphology, of the AuNRs.

The increase in the AuNR longitudinal band upon laser irradiation is expected and revealed the disruption of the CM vesicles and release of the PEG-AuNRs (Figure 3B). The release of β-Lap was estimate by dividing the sample in four aliquots, followed by irradiation for different periods and centrifugation using centrifugal filters to separate the released β-Lap from the system. The absorbance of the β-Lap at 257 nm was then measured to calculate the correspondent concentrations. The calculated released concentrations as a function of irradiation time are shown in Figure 3C. As expected, the amount of β-Lap released increases with the
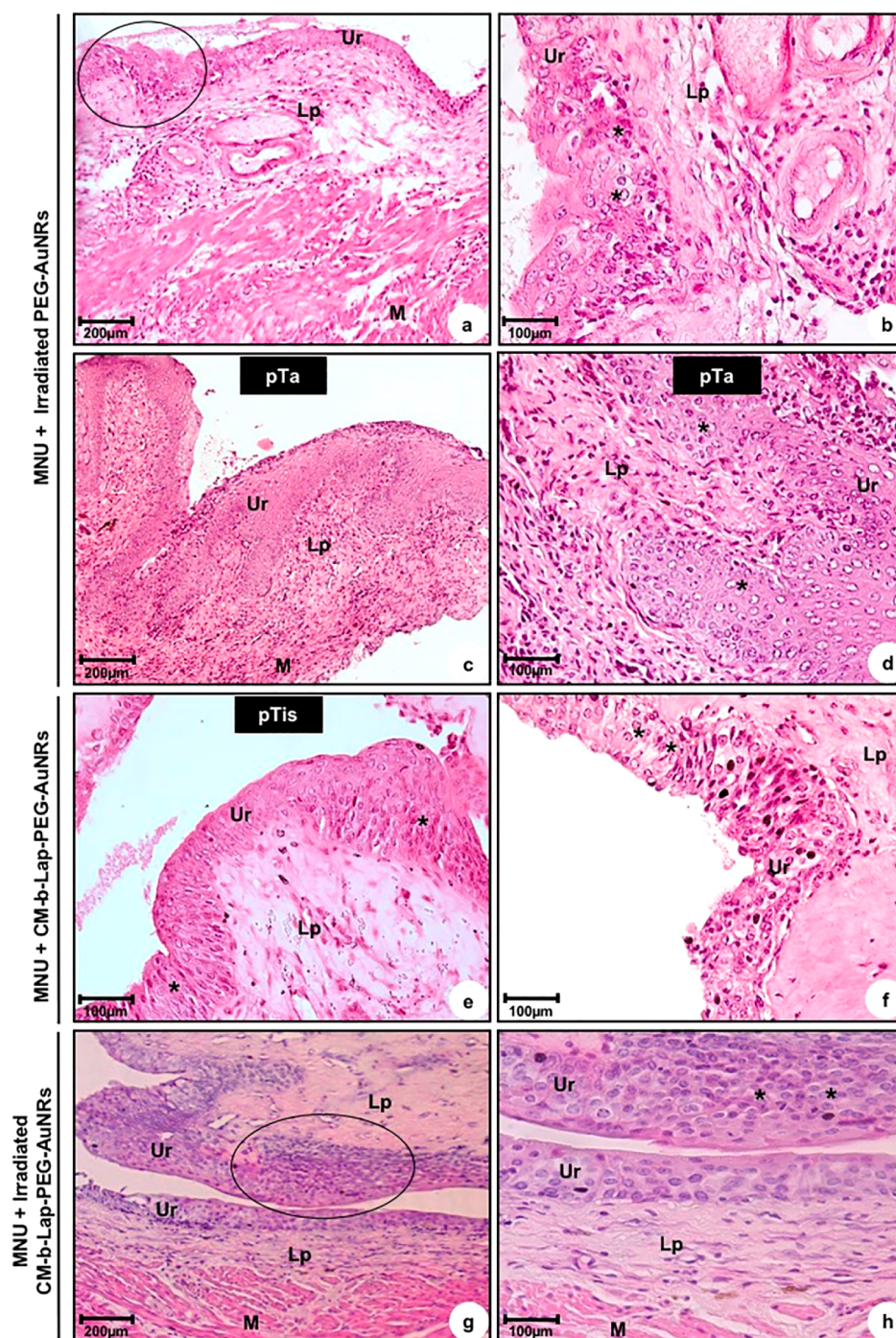
Figure 5. Representative photomicrographs of urinary bladder from (a−d) MNU + irradiated PEG-AuNR, (e, f) MNU + CM-β-Lap-PEG-AuNR, and (g, h) MNU + irradiated CM-β-Lap-PEG-AuNR groups. (a, b, f, g, h) Low-grade intraurothelial neoplasia (circle) characterized by thickening of the urothelium and presence of few atypical urothelial cells (asterisks), without loss of cell polarity. (c, d) pTa tumor: cancer cells show slender papillae with frequent branching, minimal fusion, and variations in nuclear polarity, size, shape, and chromatin pattern and with the presence of nucleoli (asterisks). (e) pTis tumor: flat lesion in the urothelium surface characterized by large and pleomorphic cells, severe nuclear atypia (asterisks) and loss of cellular polarity. a−h: Lp, lamina propria; M, muscle layer; Ur, urothelium.

irradiation time. Laser-induced release of molecules on surface of gold nanorods is a thermal process and the amount of released molecules is dependent upon the laser power and period of irradiation.[30,31] However, the total concentration of β-Lap is very low (<1.2 μM) even after 20 min of irradiation.

2.3. Enhanced Phototherapy by Cell Membrane-Coated AuNRs and β-Lap. For the in vitro photothermal therapy experiments, we used the same OD at 750 nm for both

CM-β-Lap-PEG-AuNRs and CM-PEG-AuNRs. Information about cell uptake can be found in Figures S8−S10. After 10 min of irradiation, the cells were incubated for 2 h at 37 °C and 5% CO_2, followed by staining with trypan blue to evaluate viability (Figure 4 and Figure S11). An increasing number of cells death stained by trypan blue are observed for cells treated with CM-β-Lap-PEG-AuNRs compared to the cells treated with CM-PEG-AuNRs. Because the only difference between

Table 1. Histopathological Changes in the Urinary Bladder of Rats from the Control, MNU, MNU + Irradiated PEG-AuNR, MNU + CM-β-Lap-PEG-AuNR, and MNU + Irradiated CM-β-Lap-PEG-AuNR Groups

histopathology	control (n = 4)	MNU (n = 4)	MNU + irradiated PEG-AuNRs (n = 4)	MNU + CM-b-Lap-PEG-AuNRs (n = 3)	MNU + irradiated CMb-Lap-PEG-AuNRs (n = 3)
normal	4 (100%)				
low-grade intraurothelial neoplasia			1 (25%)	1 (33.33%)	2 (66.66%)
flat carcinoma *in situ* (pTis)		2 (50%)	1 (25%)	2 (66.66%)	1 (33.33%)
papillary carcinoma *in situ* (pTa)		1 (25%)	2 (50%)		
high-grade urothelial cancer invading the lamina propria (pT1)		1 (25%)			

[a]Preneoplastic lesions, low-grade intraurothelial neoplasia; neoplastic lesions, pTis, pTa, and pT1. [b]Percentage indicates the number of animals that showed a decrease in aggressiveness and progression of bladder neoplastic lesions.

these two systems is the presence of β-Lap, we can infer that even at low concentrations (below 1.2 μM), the β-Lap is contributing for the toxicity of the CM-β-Lap-PEG-AuNRs and it has been only released after laser irradiation. It is noteworthy that only the cells in the laser spots (highlight areas) were damaged. The cytotoxicity of CM-β-Lap-PEG-AuNRs in absence of laser is shown on Supporting Information (Figure S12−S13).

2.4. Irradiated CM-β-Lap-PEG-AuNR Treatment Decreased Neoplastic Lesions Progression Induced by MNU Carcinogen. The histological observation of the animals after the cancer induction is shown on Figure S14. Normal bladder urothelium is formed by three different cell types: basal cell layer, intermediate cell layer, and surface cell layer (umbrella cells) and no histological changes were detected in bladder tissue for the control group (Figure S14A, B). In contrast, MNU group showed deep microscopic changes in the urinary bladder tissue such as flat carcinoma in situ (pTis) (Figure S14C), papillary carcinoma in situ (pTa) (Figure S14D, E) and high-grade urothelial cancer invading the lamina propria (pT1) (Figure S14F, G) in 50, 25, and 25% of the mice, respectively, similar to the results observed by Dias.[32] Some differences in the tumor bladder tissues should be highlighted. First, pTis carcinoma (Figures S14C, E) was characterized by plain lesion in the urothelium surface, showing high and pleomorphic cells, serious nuclear atypia and loss of cellular polarity. pTa tumor (Figure S14D, E and Figure 5C, D) was characterized by cancer cells showing minimal fusion, slender papillae with frequent branching, variations in nuclear polarity, size, shape, and chromatin pattern and with the presence of nucleoli. Finally, pT1 carcinoma (Figure S14F, G) was characterized by tumor cells occupying the lamina propria, numerous mitotic forms, and pleomorphic cells with extended nuclei.

Table 1 shows that the most frequent neoplastic lesions in the MNU + irradiated PEG-AuNR group were pTis and pTa (Figure 5C, D) in 25 and 50% of the animals, respectively. Low-grade intraurothelial neoplasia (Figure 5A, B) appeared in 25% of the animals, suggesting that this treatment inhibited the tumor progression in 25% of the animals. Low-grade intraurothelial neoplasia (Figure 5A, B, F, G, H) was characterized by thickening of the urothelium and presence of few atypical urothelial cells, without loss of cell polarity. The treatment with CM-β-Lap-PEG-AuNRs with no irradiation showed a decrease in aggressiveness and progression of bladder neoplastic lesions in 33.33% of the animals (Table 1). Preneoplastic lesions, such as low-grade intraurothelial neoplasia (Figure 5F), were found in 33.33% of the animals (Table 1), and the most frequent neoplastic lesion found in this group was pTis (Figure 5E) in 66.66% of the animals (Table 1).

Animals treated with CM-β-Lap-PEG-AuNRs and irradiated with laser showed superior histopathological recovery from the cancer state than those observed in the MNU + irradiated PEG-AuNR and MNU + CM-β-Lap-PEG-AuNR groups, showing a decrease in aggressiveness and progression of bladder neoplastic lesions in 66.66% of the animals (Table 1). Low-grade intraurothelial neoplasia (Figure 5G, 5H), were found in 66.66% of the animals (Table 1). The most frequent neoplastic lesion found in this group was pTis in 33.33% of the animals (Table 1).

It is noteworthy that we were able to observe a decrease in aggressiveness and progression of bladder neoplastic lesions in most animals with only one application of CM-β-Lap-PEG-AuNRs (∼1.6 × 10^{11} particles/mL, volume 100 μL) and laser irradiation for 5 min. Bladder cancer is of high incidence and standard intravesical immunotherapy and chemotherapy treatments usually require multiple applications to induce tumor regression.[33,34] These results are in agreement with the in vitro analysis and reinforce the potential of this multifunctional platform to improve cancer treatment with reduced side effects.

3. CONCLUSION

We have demonstrated the loading of PEG-AuNRs and an anticancer agent β-Lapachone into cell membranes vesicles purified from A549 cancer cells. The NIR irradiation led to disruption of the vesicles and release of the PEG-AuNRs and β-Lapachone. In vitro studies revealed the effectiveness of CM-β-Lap-PEG-AuNRs as a multifunctional agent for combined chemo and photothermal cell destruction in a synergic way. In vivo analysis revealed that animals treated with CM-b-Lap-PEG-AuNRs and NIR irradiated presented better histopathological recovery from the cancer state than those in the irradiated PEG-AuNR or nonirradiated CM-b-Lap-PEG-AuNR groups. This multifunctional platform for activated drug release and photothermia is a promising candidate for applications in cancer therapy.

4. EXPERIMENTAL SECTION

Materials. All reagents were used without further purification and the solutions were prepared using ultrapure water (Milli-Q, 18.2 MΩ cm). Cetyltrimethylammonium bromide (CTAB), silver nitrate (AgNO$_3$), tetrachloroauric acid (HAuCl$_4$), sodium borohydrate (NaBH$_4$), and ascorbic acid were purchased from Sigma-Aldrich. β-Lapachone (β-lap) and poly(ethylene glycol) methyl ether thiol (mPEG-SH) average M_n 5000 were also obtained from Sigma-Aldrich.

Gold Nanorod (AuNR) Synthesis. Gold nanorods (AuNRs) were synthesized by the seed-mediated method in the presence of the surfactant CTAB,[35] washed with chloroform to remove CTAB and subsequently functionalized with mPEG-SH. The particles were shaken for more than 12 h at room temperature and centrifuged twice (10 000 g, 5 min). The concentration of the resulting PEG-AuNRs for the experiments was standardized by their optical density at the longitudinal absorption and their extinction cross-section.[36]

Cell Culture and Extraction of A549 Cancer Cell Membrane (CM). Human lung adenocarcinoma epithelial (A549) and rat hepatocarcinoma (HTC) were acquired from Rio de Janeiro Cell Bank (BCRJ). Human hepatoma (HepaRG) cells were kindly supplied by Dra. Natalia Inada from Physics Institute of Sao Carlos, University of Sao Paulo, Brazil. All the cells lines were cultured in Dulbecco's modified Eagle's medium (DMEM) (Vitrocell) supplemented with 10% of fetal bovine serum (Vitrocell) and maintained at 37 °C and in 5% CO_2 in a humidified incubator.

The A549 cancer cell membranes were isolated and purified by ultracentrifugation based on a previous method proposed by Lung et al.[37] and reconstructed as vesicles by extrusion. The membrane was characterized by sodium dodecyl sulfate polyacrylamide 10% gel electrophoresis (SDS-PAGE). The standard BenchMark Protein Ladder (Invitrogen) was used as reference for mass determination and the gel was fixed and stained with silver nitrate (ProteoSilver kit, Sigma-Aldrich). The quantitative determination of protein in the cell membrane was performed by the QuantiPro BCA Assay Kit (Sigma-Aldrich). The procedure was carried out according to the described at the assay's protocol. First, a calibration curve was obtained using known concentrations of bovine serum albumin (BSA) (Figure S15) and then different concentrations of the cell membrane were measured, and the concentration determined from the calibration curve.

The lipid composition of the cell membrane was analyzed by Iatroscan TLC/FID (Iatroscan MK-VI, Iatron, Japan).[38] The lipids standards HC (aliphatic hydrocarbons), WE/SE (ester), TAG (triglycerides), FFA (free fatty acids), ALC (aliphatic alcohol free), ST (sterol), AMPL (mobile polar lipids in ketone), and PL (phospholipids) were obtained from Sigma-Aldrich and all other chemicals and solvents were of analytical grade. For this analysis, the A549 cell membranes were resuspended in chloroform after ultracentrifugation using the same volume as previously described for the buffer. Before the Iatroscan analysis, the samples were homogenized in a bath ultrasound at 4 °C for 15 min. The lipids samples were resolved in three steps, which involved subsequent elutions in solvent mixtures with increased polarity, as follows: (i) 98.95% hexane, 1% diethyl ether, and 0.05% formic acid (solution 1); (ii) 79% hexane, 20% diethyl ether, and 1% formic acid (solution 2); (iii) 100% acetone (solution 3); and (iv) 50% chloroform, 40% methanol, and 10% water (solution 4).

A549 Cell Membrane-Loaded β-Lapachone (CM-β-Lap). The cell membrane with a protein concentration of 774.9 $\mu g\ mL^{-1}$ was sonicated in an ice bath sonicator at 4 °C for 15 min. β-Lap (0.07 mg, ∼ 0.3 mmol L^{-1}) was then added to the system and the system was sonicated again, followed by gentle shaken for 2 h at 4 °C and protected from light. The system was extruded through 200 nm polycarbonate membrane using a miniextruder (Avanti Polar Lipids), dialyzed against 0.2x PBS buffer at 4 °C, protected from light, for 3 h to remove the remnants from cell-membrane extraction and the excess of β-Lap. The resulting suspension was collected and kept at 4 °C.

CM-β-Lap-Coated PEG-Gold Nanorods (CM-β-Lap-PEG-AuNRs). The CM/AuNR ratio was tested and optimized to promote surface stability. The CM-β-Lap suspension was extruded 11 times through 200 nm polycarbonate membrane using a miniextruder (Avanti Polar Lipids), followed by additional 7 extrusions using a 100 nm membrane. The size and distribution of the extruded membranes were evaluated by dynamic light scattering (DLS) (Zerasizer Nano ZS, Malvern). 500 μL of CM-β-Lap suspension was added to 2000 μL of PEG-AuNRs (∼1.6 × 10^{11} particles/mL) and extruded 7 times through a 100 nm polycarbonate membrane. The system was

centrifuged (5000 g, 10 min) to remove the excess of membrane or β-Lap, and the particles were resuspended in PBS.

The loading concentration of β-lap in the final system was determined by destabilization of the cell membrane to release the anticancer agent. In this case, CM-β-lap-PEG-AuNRs were diluted in ethanol and sonicated for 30 min. The particles were centrifuged at 10000g for 15 min and the supernatant spectrum was measured using an UV−VIS spectrophotometer (Hitachi U-2900). The β-Lap concentration was estimated using the extinction coefficient calculated from the calibration curve (Figure S16).

For comparison, we also synthesized A549 cell membrane-coated PEG-functionalized gold nanorods (CM-PEG-AuNRs), i.e., without β-lap, using the same procedure as described for CM-β-Lap-PEG-AuNRs. The concentration of free PEG-AuNRs, CM-PEG-AuNRs, and CM-β-Lap-PEG-AuNRs was estimated using the longitudinal absorption and the extinction cross section of the gold nanorods.[36]

Characterization. The optical properties of the PEG-AuNRs before and after conjugation with CM-β-Lap were characterized by UV−vis−NIR spectroscopy (Hitachi U-2900). Their size, distribution, and morphology, before and after laser irradiation, were analyzed by scanning electron microscopy (Zeiss Sigma VP FEG-SEM) at 3 kV. In this case, silicon substrates (P-type/boron-doped silicon, Sigma-Aldrich) were cleaned with isopropanol, ethanol, and water in an ultrasound bath (2 min each) and dried in a stream of nitrogen gas. The samples were diluted in water, drop-cast onto the substrate and allowed to dry in ambient conditions for 12 h.

Dynamic light scattering (DLS) was used to evaluate hydrodynamic diameter and distribution of the samples in suspension. The measurements were performed in triplicate at room temperature using a Malvern spectrometer Nano-ZS (Marvern Instruments). The zeta potential of the AuNRs after each step of functionalization was also evaluated using a Malvern spectrometer Nano-ZS (Marvern Instruments). The results are presented as mean ± SD resulting from three different measurements. Serum stability of the resulting CM-β-Lap-PEG-AuNRs was investigated by resuspending the nanomaterials in 1x PBS and 100% FBS solution and monitoring their hydrodynamic diameter by DLS. All samples were incubated at 37 °C and gentle shacked prior to measurements

In Vitro Photothermal therapy. The optical properties of the CM-β-Lap-PEG-AuNRs were analyzed and compared with the PEG-AuNRs. 700 μL of each system (∼1.6 × 10^{11} gold nanorods/mL for the PEG-AuNRs) in a 3 mL polystyrene cuvette were irradiated using a cw diodo 808 nm laser with elliptical beam of diameter ∼1.5 mm × 3.0 mm (iZi, LASERline). The power at the distance of irradiation was measured and adjusted to a power density of 1.5 W cm^{-2}. The temperature was monitored using an optical thermometer (FOT Lab Kit Fluoptic Thermometer, LUXTRON). The initial temperature was the laboratory room temperature (∼23 °C).

The release of β-Lap was determined based on previous methods.[22] Briefly, the final CM-β-Lap-PEG-AuNR sample was divided in four aliquots (400 μL each), irradiated with the laser with a power density of 1.5 W cm^{-2} for different times (5, 10, 15, 20 min), and centrifuged immediately to separate the released β-Lap from the particles at (5000 g, 10 min at 4 °C) using a Microcon centrifugal filters (MW cutoff = 10 kDa). Typical absorbance of the β-Lap at 257 nm was measured in the resulting filtrate and used to calculate its release concentration, based on the calibration curve shown in Figure S16.

For the in vitro photothermal analysis, 5 × 10^{4} A549 cells were seed in a 96-well plate. After 24 h, the media was removed and 140 μL of media containing PBS (control), CM-β-Lap-PEG-AuNRs or CM-PEG-AuNRs were added to each well in triplicate. We use the absorbance at the maximum longitudinal peak to standardize the concentrations of both systems. The final particle concentration in cell culture media was ∼8.2 × 10^{10} particles/mL. The cells were incubated for 4 h at 37 °C and 5% CO_2 and washed twice with PBS. Finally, 100 μL of media were added to each well and the cells were irradiated using the same cw diodo 808 nm laser with elliptical beam of diameter ∼1.5 mm × 3.0 mm (iZi, LASERline) and power density was also adjusted to have approximately 1.5 W cm^{-2}. After exposing to the laser light for 10 min, the cells were incubated for an additional 2 h at

37 °C and 5% CO_2, followed by staining with 0.4% trypan blue (Sigma-Aldrich) to evaluate the viability. The images were taken using an inverted light Zeiss microscope.

Nonmuscle Invasive Bladder Cancer (NMIBC) Induction and Photothermal Therapy. Eighteen female C57BL/6 mice 7 weeks old were obtained from the Multidisciplinary Center for Biological Investigation (CEMIB) at the University of Campinas (UNICAMP). The animal experiments were approved by an institutional Committee for Ethics in Animal Use (CEUA/UNICAMP, protocol no. 4413−1). The tumor induction was performed according to Dias,[32] being that four mice were used as control groups and another 14 mice were used for NMIBC induction. After the induction protocol, all mice were submitted to ultrasonography to check the existence of the tumors.

For both systems PEG-AuNRs and CM-β-Lap-PEG-AuNRs, the samples were prepared in phosphate buffer at ~1.6 × 10^{11} particles/ mL (for PEG-AuNRs). The irradiation was performed using a cw diodo 808 nm laser with elliptical beam of diameter ~1.5 mm × 3.0 mm (iZi, LASERline) and power density adjusted to approximately 1 W cm^{-2}. MNU-treated rats were divided into four groups: (1) MNU group (n = 4 animals) received 100 μL single dose of 0.9% physiological saline, intravesically; (2) MNU + PEG-AuNR irradiated group (n = 4 animals) received 100 μL single dose of PEG-AuNRs, intravesically, and irradiated for 5 min; (3) MNU + CM-b-Lap-PEG-AuNR group (n = 3 animals) received 100 μL single dose of CM-b-Lap-PEG-AuNRs, intravesically; and (4) MNU + CM-b-Lap-PEG-AuNR irradiated group (n = 3 animals) received 100 μL single dose of CM-b-Lap-PEG-AuNRs, intravesically, and irradiated for 5 min. Two weeks after the therapeutic dose instillation, the urinary bladders from treated and untreated mice were collected and processed for histopathological analysis according to protocol performed by Dias.[32]

■ ASSOCIATED CONTENT

Ⓢ Supporting Information

The Supporting Information is available free of charge on the ACS Publications website at DOI: 10.1021/acsabm.8b00603.

Additional information on materials characterization and experimental procedures (PDF)

■ AUTHOR INFORMATION

Corresponding Author
*Email: zuco@ifsc.usp.br.

ORCID Ⓘ
Valeria S. Marangoni: 0000-0002-3732-504X
Juliana Cancino Bernardi: 0000-0002-9584-2248
Valtencir Zucolotto: 0000-0003-4307-3077

Notes
The authors declare no competing financial interest.

■ ACKNOWLEDGMENTS

■ REFERENCES

(1) O'Neal, D. P.; Hirsch, L. R.; Halas, N. J.; Payne, J. D.; West, J. L. Photo-Thermal Tumor Ablation in Mice Using near Infrared-Absorbing Nanoparticles. *Cancer Lett.* **2004**, *209* (2), 171−176.

(2) Weissleder, R. A Clearer Vision for in Vivo Imaging: Progress Continues in the Development of Smaller, More Penetrable Probes for Biological Imaging. *Nat. Biotechnol.* **2001**, *19* (4), 316−317.

(3) Dickerson, E. B.; Dreaden, E. C.; Huang, X.; El-Sayed, I. H.; Chu, H.; Pushpanketh, S.; McDonald, J. F.; El-Sayed, M. A. Gold Nanorod Assisted Near-Infrared Plasmonic Photothermal Therapy (PPTT) of Squamous Cell Carcinoma in Mice. *Cancer Lett.* **2008**, *269* (1), 57−66.

(4) Ali, M. R. K.; Wu, Y.; Tang, Y.; Xiao, H.; Chen, K.; Han, T.; Fang, N.; Wu, R.; El-Sayed, M. A. Targeting Cancer Cell Integrins Using Gold Nanorods in Photothermal Therapy Inhibits Migration through Affecting Cytoskeletal Proteins. *Proc. Natl. Acad. Sci. U. S. A.* **2017**, *114* (28), E5655−E5663.

(5) Abadeer, N. S.; Murphy, C. J. Recent Progress in Cancer Thermal Therapy Using Gold Nanoparticles. *J. Phys. Chem. C* **2016**, *120* (9), 4691−4716.

(6) Liao, J.; Li, W.; Peng, J.; Yang, Q.; Li, H.; Wei, Y.; Zhang, X. Combined Cancer Photothermal-Chemotherapy Based on Doxorubicin/Gold Nanorod-Loaded Polymersomes. *Theranostics* **2015**, *5* (4), 345−356.

(7) Parodi, A.; Quattrocchi, N.; Van De Ven, A. L.; Chiappini, C.; Evangelopoulos, M.; Martinez, J. O.; Brown, B. S.; Khaled, S. Z.; Yazdi, I. K.; Enzo, M. V.; Isenhart, L.; Ferrari, M.; Tasciotti, E. Synthetic Nanoparticles Functionalized with Biomimetic Leukocyte Membranes Possess Cell-like Functions. *Nat. Nanotechnol.* **2013**, *8* (1), 61−68.

(8) Hu, C.-M. J.; Zhang, L.; Aryal, S.; Cheung, C.; Fang, R. H.; Zhang, L. Erythrocyte Membrane-Camouflaged Polymeric Nanoparticles as a Biomimetic Delivery Platform. *Proc. Natl. Acad. Sci. U. S. A.* **2011**, *108* (27), 10980−10985.

(9) Hu, C.-M. J.; Fang, R. H.; Luk, B. T.; Chen, K. N. H.; Carpenter, C.; Gao, W.; Zhang, K.; Zhang, L. Marker-of-Self Functionalization of Nanoscale Particles through a Top-down Cellular Membrane Coating Approach. *Nanoscale* **2013**, *5* (7), 2664−2668.

(10) Gao, W.; J, H. C.; H, F. R.; T, L. B.; Jing, S.; Liangfang, Z. Surface Functionalization of Gold Nanoparticles with Red Blood Cell Membranes. *Adv. Mater.* **2013**, *25* (26), 3549−3553.

(11) Piao, J.-G.; Wang, L.; Gao, F.; You, Y.-Z.; Xiong, Y.; Yang, L. Erythrocyte Membrane Is an Alternative Coating to Polyethylene Glycol for Prolonging the Circulation Lifetime of Gold Nanocages for Photothermal Therapy. *ACS Nano* **2014**, *8* (10), 10414−10425.

(12) Brähler, M.; Georgieva, R.; Buske, N.; Müller, A.; Müller, S.; Pinkernelle, J.; Teichgräber, U.; Voigt, A.; Bäumler, H. Magnetite-Loaded Carrier Erythrocytes as Contrast Agents for Magnetic Resonance Imaging. *Nano Lett.* **2006**, *6* (11), 2505−2509.

(13) Fang, R. H.; Hu, C.-M. J.; Luk, B. T.; Gao, W.; Copp, J. A.; Tai, Y.; O'Connor, D. E.; Zhang, L. Cancer Cell Membrane-Coated Nanoparticles for Anticancer Vaccination and Drug Delivery. *Nano Lett.* **2014**, *14* (4), 2181−2188.

(14) Shao, K.; Singha, S.; Clemente-Casares, X.; Tsai, S.; Yang, Y.; Santamaria, P. Nanoparticle-Based Immunotherapy for Cancer. *ACS Nano* **2015**, *9* (1), 16−30.

(15) Kim, H.; Lee, J.; Oh, C.; Park, J. H. Cooperative Tumour Cell Membrane Targeted Phototherapy. *Nat. Commun.* **2017**, *8*, 15880.

(16) Toledano Furman, N. E.; Lupu-Haber, Y.; Bronshtein, T.; Kaneti, L.; Letko, N.; Weinstein, E.; Baruch, L.; Machluf, M. Reconstructed Stem Cell Nanoghosts: A Natural Tumor Targeting Platform. *Nano Lett.* **2013**, *13* (7), 3248−3255.

(17) Bahmani, B.; Bacon, D.; Anvari, B. Erythrocyte-Derived Photo-Theranostic Agents: Hybrid Nano-Vesicles Containing Indocyanine Green for near Infrared Imaging and Therapeutic Applications. *Sci. Rep.* **2013**, *3*, 1−7.

(18) Hirlekar, R.; Patel, P.; Dand, N.; Kadam, V. Drug Loaded Erythrocytes: As Novel Drug Delivery System. *Curr. Pharm. Des.* **2008**, *14* (1), 63−70.

(19) Gupta, N.; Patel, B.; Ahsan, F. Nano-Engineered Erythrocyte Ghosts as Inhalational Carriers for Delivery of Fasudil: Preparation and Characterization. *Pharm. Res.* **2014**, *31* (6), 1553−1565.

(20) Pink, J. J.; Planchon, S. M.; Tagliarino, C.; Varnes, M. E.; Siegel, D.; Boothman, D. A. NAD(P)H: Quinone Oxidoreductase Activity Is the Principal Determinant of β-Lapachone Cytotoxicity. *J. Biol. Chem.* **2000**, *275* (8), 5416−5424.

(21) Zhang, L.; Chen, Z.; Yang, K.; Liu, C.; Gao, J.; Qian, F. β-Lapachone and Paclitaxel Combination Micelles with Improved Drug Encapsulation and Therapeutic Synergy as Novel Nanotherapeutics

for NQO1-Targeted Cancer Therapy. *Mol. Pharmaceutics* **2015**, *12* (11), 3999−4010.

(22) Blanco, E.; Bey, E. A.; Dong, Y.; Weinberg, B. D.; Sutton, D. M.; Boothman, D. A.; Gao, J. β-Lapachone-Containing PEG−PLA Polymer Micelles as Novel Nanotherapeutics against NQO1-Overexpressing Tumor Cells. *J. Controlled Release* **2007**, *122* (3), 365−374.

(23) Blanco, E.; Bey, E. A.; Khemtong, C.; Yang, S.-G.; Setti-Guthi, J.; Chen, H.; Kessinger, C. W.; Carnevale, K. A.; Bornmann, W. G.; Boothman, D. A.; Gao, J. β-Lapachone Micellar Nanotherapeutics for Non-Small Cell Lung Cancer Therapy. *Cancer Res.* **2010**, *70* (10), 3896−3904.

(24) Rao, J. S.; Gondi, C.; Chetty, C.; Chittivelu, S.; Joseph, P. A.; Lakka, S. S. Inhibition of Invasion, Angiogenesis, Tumor Growth, and Metastasis by Adenovirus-Mediated Transfer of Antisense UPAR and MMP-9 in Non{\textendash}small Cell Lung Cancer Cells. *Mol. Cancer Ther.* **2005**, *4* (9), 1399−1408.

(25) Tan, S.; Wu, T.; Zhang, D.; Zhang, Z. Cell or Cell Membrane-Based Drug Delivery Systems. *Theranostics* **2015**, *5* (8), 863−881.

(26) Nghiem, T. H. L.; La, T. H.; Vu, X. H.; Chu, V. H.; Nguyen, T. H.; Le, Q. H.; Fort, E.; Do, Q. H.; Tran, H. N. Synthesis, Capping and Binding of Colloidal Gold Nanoparticles to Proteins. *Adv. Nat. Sci.: Nanosci. Nanotechnol.* **2010**, *1* (2), 025009.

(27) Wang, L.; Yingyue, Z.; Liguang, X.; Wei, C.; Hua, K.; Liqiang, L.; Ashish, A.; Chuanlai, X.; A, K. N. Side-by-Side and End-to-End Gold Nanorod Assemblies for Environmental Toxin Sensing. *Angew. Chem., Int. Ed.* **2010**, *49* (32), 5472−5475.

(28) Özcan, I.; Segura-Sánchez, F.; Bouchemal, K.; Sezak, M.; Özer, Ö.; Güneri, T.; Ponchel, G. Pegylation of Poly(γ-Benzyl-L-Glutamate) Nanoparticles Is Efficient for Avoiding Mononuclear Phagocyte System Capture in Rats. *Int. J. Nanomed.* **2010**, *5* (1), 1103−1111.

(29) Martínez-Barbosa, M. E.; Cammas-Marion, S.; Bouteiller, L.; Vauthier, C.; Ponchel, G. PEGylated Degradable Composite Nanoparticles Based on Mixtures of PEG-b-Poly(γ-Benzyl l-Glutamate) and Poly(γ-Benzyl l-Glutamate). *Bioconjugate Chem.* **2009**, *20* (8), 1490−1496.

(30) Huschka, R.; Zuloaga, J.; Knight, M. W.; Brown, L. V.; Nordlander, P.; Halas, N. J. Light-Induced Release of DNA from Gold Nanoparticles: Nanoshells and Nanorods. *J. Am. Chem. Soc.* **2011**, *133* (31), 12247−12255.

(31) Yamashita, S.; Fukushima, H.; Akiyama, Y.; Niidome, Y.; Mori, T.; Katayama, Y.; Niidome, T. Controlled-Release System of Single-Stranded DNA Triggered by the Photothermal Effect of Gold Nanorods and Its in Vivo Application. *Bioorg. Med. Chem.* **2011**, *19* (7), 2130−2135.

(32) Dias, L. P.; Luzo, Â. C. M.; Volpe, B. B.; Durán, M.; Galdames, S. E. M.; Ferreira, L. A. B.; Durán, N.; Fávaro, W. J. Effects of Intravesical Therapy with Platelet-Rich Plasma (PRP) and Bacillus Calmette-Guérin (BCG) in Non-Muscle Invasive Bladder Cancer. *Tissue Cell* **2018**, *52*, 17−27.

(33) Askeland, E. J.; Newton, M. R.; O'Donnell, M. A.; Luo, Y. Bladder Cancer Immunotherapy: BCG and Beyond. *Adv. Urol.* **2012**, *2012*, No. 181987.

(34) Reis, L. O.; Ferreira, U.; Billis, A.; Cagnon, V. H. A.; Fávaro, W. J. Anti-Angiogenic Effects of the Superantigen Staphylococcal Enterotoxin B and Bacillus Calmette-Guérin Immunotherapy for Nonmuscle Invasive Bladder Cancer. *J. Urol.* **2012**, *187* (2), 438−445.

(35) Sau, T. K.; Murphy, C. J. Seeded High Yield Synthesis of Short Au Nanorods in Aqueous Solution. *Langmuir* **2004**, *20* (15), 6414−6420.

(36) Chon, J. W. M.; Bullen, C.; Zijlstra, P.; Gu, M. Spectral Encoding on Gold Nanorods Doped in a Silica Sol−Gel Matrix and Its Application to High-Density Optical Data Storage. *Adv. Funct. Mater.* **2007**, *17* (6), 875−880.

(37) Lund, R.; Leth-Larsen, R.; Jensen, O. N.; Ditzel, H. J. Efficient Isolation and Quantitative Proteomic Analysis of Cancer Cell Plasma Membrane Proteins for Identification of Metastasis-Associated Cell Surface Markers. *J. Proteome Res.* **2009**, *8* (6), 3078−3090.

(38) De Schrijver, R.; Vermeulen, D. Separation and Quantitation of Phospholipids in Animal Tissues by Latroscan TLC/FID. *Lipids* **1991**, *26* (1), 74−76.